AIP | Review of Scientific Instruments

Recent progress of white light interferometric fiberoptic strain sensing techniques

Libo Yuan, Limin Zhou, Wei Jin, and C. C. Chan

Citation: Rev. Sci. Instrum. **71**, 4648 (2000); doi: 10.1063/1.1324736
View online: http://dx.doi.org/10.1063/1.1324736
View Table of Contents: http://rsi.aip.org/resource/1/RSINAK/v71/i12
Published by the American Institute of Physics.

Recent progress of white light interferometric fiberoptic strain sensing techniques

Libo Yuan[a)]
Department of Physics, Harbin Engineering University, Harbin 150001, People's Republic of China

Limin Zhou
Department of Mechanical Engineering, The Hong Kong Polytechnic University, Hong Kong, People's Republic of China

Wei Jin and C. C. Chan
Department of Electrical Engineering, The Hong Kong Polytechnic University, Hong Kong, People's Republic of China

(Received 7 February 2000; accepted for publication 18 September 2000)

Strain, deformation, and temperature measurements constitute some of the most interesting parameters to be monitored in composite materials or structures. White light interferometry offers good performance even for long-term measurements of these parameters. Based on the Michelson interferometer, a fiberoptic localized extensometer and multiplexing strain-sensing techniques are demonstrated in this article. Related problems such as the effect of optical fiber coating on an embedded sensor and the dual use of one sensor are discussed. Finally, application examples of surface strain and internal strain (0–6000 microstrain) and temperature (22–36 °C) of concrete sample are given. © *2000 American Institute of Physics.* [S0034-6748(00)04312-4]

I. INTRODUCTION

The use of embedded optical fiber in composite and concrete structures has been pursued over the past 20 years for material evaluation or strain monitoring.[1] For located strain or distributed strain measurement, individual optical fiber segments can be embedded in the composites, for instance, concrete, to map the condition of the structure at any time. A range of optical fiber versions of classical interferometer configurations, such as the two-beam Michelson, Mach–Zehnder, and Fabry-Pérot interferometer have been used in this field.[2] This article, however, concentrates on our recent works in white light interferometric strain sensors for smart materials and structures based on two-beam interferometric configurations, mainly the Michelson interferometer.

II. INTERACTION BETWEEN COATED FIBEROPTIC SENSOR GAUGE AND HOST MATERIALS

Fiberoptic sensors operating on interferometric principles have been considered for measuring strains and deformation inside composite materials or concrete structures. Owing to the complex interactions between the sensor output and the strains inside the host materials, strain cannot be determined by simple tests. In general, the relationships providing the bridge between the sensor output and the engineering values of the strains must be established via analytical models.

The simplest fiberoptic sensor is a length of fiber with two reflective end surfaces as shown in Fig. 1; it consists of a core, a cladding and a coating. The coating is provided to protect the glass optical fiber from breaking in practical applications. A length of optical fiber as a sensor is embedded inside the material and then it disturbs the strain field. We wish to measure those strains, which would exist at the location of the sensor in the absence of the sensor. This can be accomplished by realizing that at a short distance from the sensor, the strains are nearly the same as those which would exist at the location of the sensor in the absence of the sensor. These strains are referred to as far-field strains.

Optical fiber sensors are either structurally embedded during production of elements or attached to the surface of the test piece by way of adhesives. When a fiberoptic sensor is embedded in the composite material or a structure as shown in Fig. 2, in which the strain is to be measured, deformation or microcrack of the matrix material, see Figs. 3 and 4, will induce changes in the optical fiber.

Elongation of the fiber divided by the fiber gauge length and the equivalent refractive index indicates fiber strain. If the matrix-glass fiber bond were perfect, then the two materials would be equally sensitive to the imposed strain. That is, the strain in the glass fiber would be equal to the strain in the surrounding matrix. However, in practice, the fiber optic has a polymer coating. If the coating is far less rigid than the

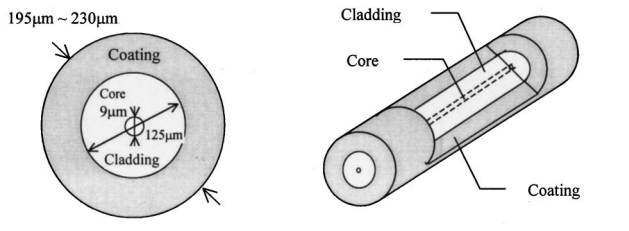

FIG. 1. Structure illustrations of an embedded optical fiber sensor gauge.

[a)]Electronic mail: liboyuan@usa.net

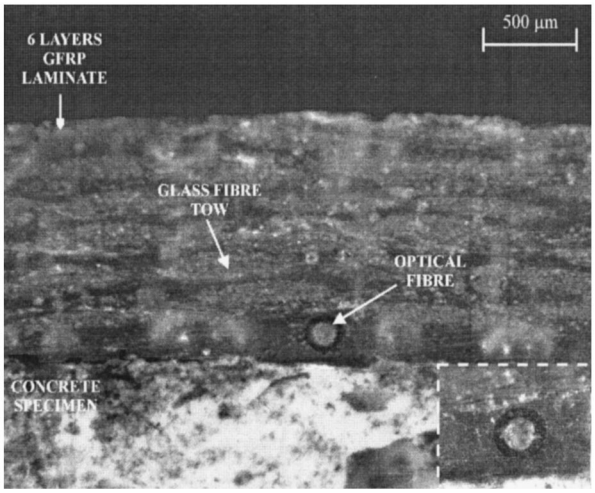

FIG. 2. Polished cross section of coated optical fiber embedded in the composite material.

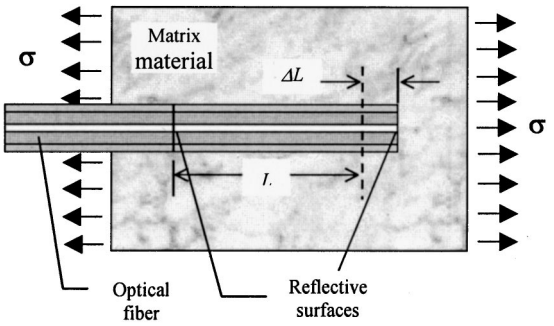

FIG. 3. Embedded fiberoptic sensor measuring strain.

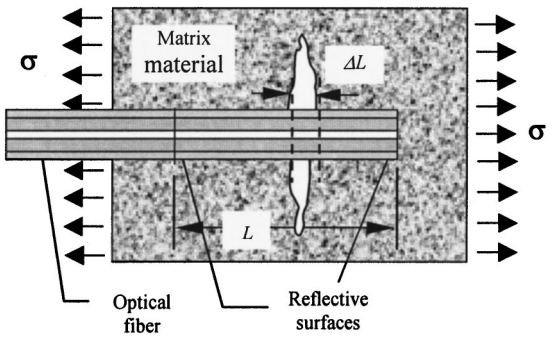

FIG. 4. Embedded fiberoptic sensor monitoring crack.

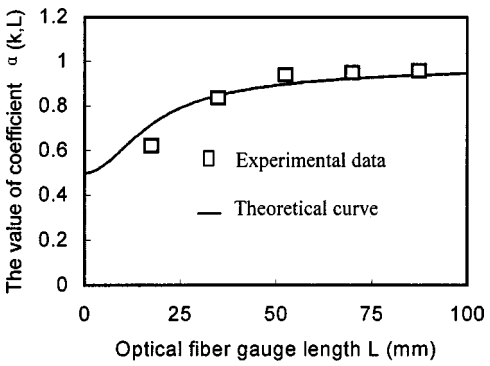

FIG. 5. Coefficient $\alpha(k,L)$ vs optical fiber gauge length L.

glass fiber and surrounding matrix material, then, even with a perfect matrix-fiber bond, the layered cross section is expected to affect the performance of the fiber sensor. The interaction between uncoated bare fiber and the matrix have been considered in Refs. 3–6 and the effects of the coating for fiberoptic sensors embedded in isotropic materials and subjected to axisymmetric loading conditions have been examined in Refs. 6–10. These authors presented closed form solutions, which related the far-field strains to the sensor strains. Transverse nonaxisymmetric loading conditions have been studied in Refs. 11–14 and under the transversely isotropic materials subjected to nonaxisymmetric loading conditions have been investigated in Ref. 15. Here, a simple model has been developed for evaluation of the strain response of a length of coated optical fiber embedded in host material.[16,17] The strain distribution along the fiber is given by Eq. (1) and the relationship between the average strain of a length of embedded fiber and the host material strain is calculated as shown in Eq. (2). Here, $\alpha(k,L)$ is the coefficient, which depends on the coating material related parameter k and embedded optical fiber length. Compared with the theoretical curve, the experimental results for different gauge length of fiber optic are also shown in Fig. 5.

$$\epsilon_{\text{fiber}}(z)=\epsilon_{\text{host-material}}\left[1-\frac{\sinh(kz)}{\sinh(kL)}\right], \tag{1}$$

$$\overline{\epsilon}_{\text{fiber}}(z)=\alpha(k,L)\,\epsilon_{\text{host-material}}, \tag{2}$$

$$\alpha(k,L)=\left[1-\frac{\cosh(kL)-1}{kL\sinh(kL)}\right]. \tag{3}$$

III. WHITE LIGHT INTERFEROMETRIC FIBEROPTIC STRAIN SENSOR MEASURING PRINCIPLE

A fiberoptic Michelson interferometer operates by a well-established technique.[18–21] Two beams are reflected and recombined on a Michelson configuration, shown in Fig. 6. When the optical-path difference between these two beams falls to within the coherence length of the light source, a white light interference fringe pattern is produced (see Fig. 7). The central fringe, which is located in the center of the fringe pattern and has the highest amplitude, corresponds to the exact optical path of these two beams. This technique can be utilized as a powerful tool for the measurement of deformations and strains that affect the optical path. In Fig. 6, the system is comprised of a light-emitting diode, center wave-

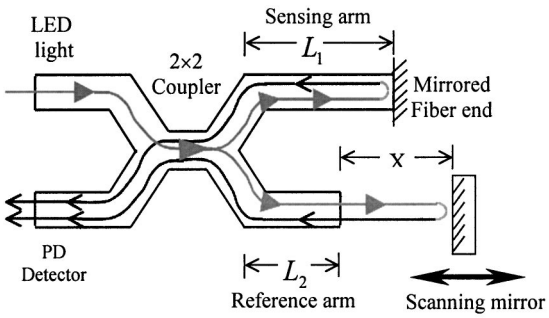

FIG. 6. Fiberoptic white light Michelson interferometer.

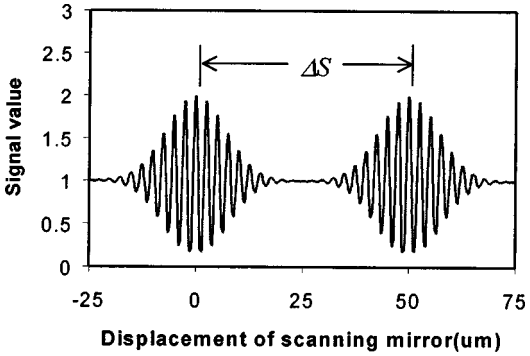

FIG. 7. Illustration of fringe pattern shift corresponding to the fiberoptic sensor gauge length elongation.

length 1300 nm, a fiberoptic coupler for separating and recombining the light, two optical arms, and a scanning mirror mounted on a translation stage. The length of the fiberoptic sensor arm is fixed, and the reference arm made slightly shorter than the sensing arm.

The reflective surfaces in both of the optical fibers guide the light back to a detector by way of a coupler. The sensing arm is embedded in the test specimen. In the unloaded position the mirror scans a short distance in front of the reference arm. Once the sum of the scanned distance and the length of the reference arm equals that of the sensing arm, white light fringes similar to those shown in Fig. 7 appear. The zero-order fringe, which is approximately in the center of the fringe pattern and has the highest amplitude, corresponds to the exact optical path matching of these two beams. This procedure can be repeated for locating the new white light fringe pattern due to straining of the sensing arm. As shown in Fig. 7, the distance between the zero-order fringe patterns for the undeformed and deformed positions gives the amount of optical path change in gauge length L. The procedure of successive deformations can be measured by way of automation. The displacement of the mirror is equal to the optical path length change of the fiber with the gauge length L; it can be expressed as

$$dS = n dL(\epsilon) + dn(\epsilon) L, \tag{4}$$

where dS is the displacement of the mirror. The first term $dL(\epsilon)$ in Eq. (4) represents the physical change of optical fiber length produced by the strain, it is directly related to the axial strain ϵ through the expression

$$dL(\epsilon) = L\epsilon. \tag{5}$$

The second term in Eq. (4), the change in optical path length due to a change in the refractive index of the fiber core, is given by[22]

$$dn = \tfrac{1}{2} n^3 [(1-\mu) p_{12} - \mu p_{11}] \epsilon. \tag{6}$$

Thus, we have

$$\begin{aligned} dS &= \{ nL\epsilon - \tfrac{1}{2} n^3 [(1-\mu) p_{12} - \mu p_{11}] L\epsilon \} \\ &= \{ n - \tfrac{1}{2} n^3 [(1-\mu) p_{12} - \mu p_{11}] \} L\epsilon \\ &= n_{\text{equivalent}} L\epsilon, \end{aligned} \tag{7}$$

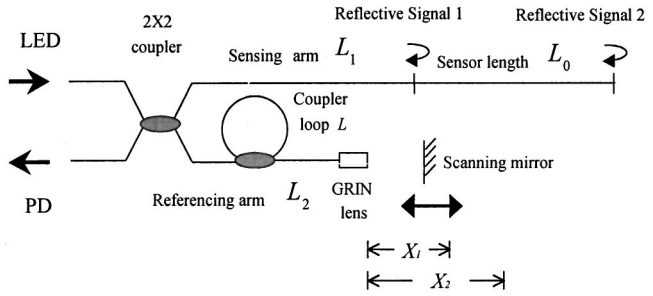

FIG. 8. Michelson white light interferometer based fiberoptic extensometer measuring principle.

where $n_{\text{equivalent}} = n - \frac{1}{2} n^3 [(1-\mu) p_{12} - \mu p_{11}]$ represents the equivalent refractive index of the fiber core. For silica materials at wavelength $\lambda = 1300\,\text{nm}$, the parameters are $n = 1.46$, Poisson ratio $\mu = 0.25$, and photoelastic constants $p_{11} = 0.12$ and $p_{12} = 0.27$, taken from Ref. 23. Using these data, the equivalent index can be calculated as $n_{\text{equivalent}} = 1.19$. Therefore, the strain on the optical fiber can be determined from

$$\epsilon = \frac{dS}{n_{\text{equlvalent}} L}. \tag{8}$$

IV. DEVELOPMENT OF LOCALIZED WHITE LIGHT INTERFEROMETRIC FIBEROPTIC EXTENSOMETER

The fiberoptic extensometer is based on a Michelson white light interferometer.[24] Its working principle is shown in Fig. 8. Light travels along the sensing arm L_1. A fraction is reflected at the first reflective surface of the sensing gauge; this is optical signal 1. The path length of the other beam is referencing arm L_2 plus the distance X_1, which can be changed by adjusting the scanning mirror. The optical signal reflected from the scanning mirror and the sensor's first reflective surface are recombined. If the path length of the referencing variable arm of light is made equal to that of the sensing arm, then the first white light interference pattern is generated. The central fringe corresponds to the exact optical path matching of these two arms. Similar to the above process, the sensing beam traverses sensing arm L_1 and through the first and second surface of the sensing gauge L_0, where it is reflected, generating a reflective signal 2. This signal recombines with the signal from the scanning mirror and the optical path through the referencing arm L_2 plus the half of coupler loop length $L/2$ and the scanning distance X_2 as shown in Fig. 8. Thus, we get the second white light interference pattern.

Assuming that the sensing fiber arm and the reference fiber arm length are L_1 and L_2, and the fiberoptic extensometer gauge length is L_0, then the first length-equilibrium equation can be written as

$$2L_1 n = 2L_2 n + 2X_1, \tag{9}$$

where, X_1 is the distance between the GRIN lens end of reference fiber and scanning mirror. Similarly, the second optical path length-equilibrium equation is

$$2L_1 n + 2L_0 n = 2L_2 n + Ln + 2X_2. \tag{10}$$

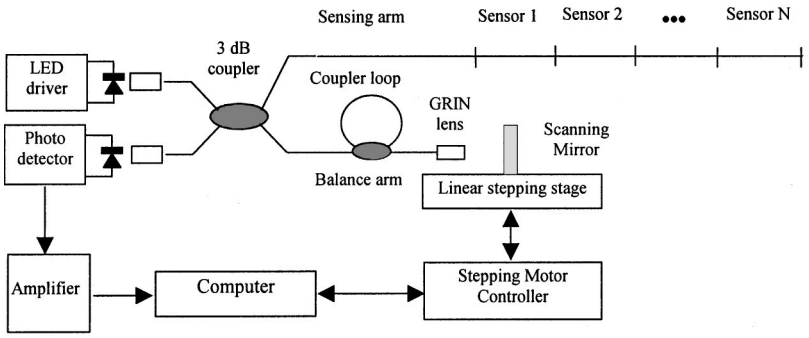

FIG. 9. Multiplexing fiberoptic strain sensing system using a fiberoptic coupler loop.

Using Eq. (10) minus Eq. (9), we have

$$(L_0-\tfrac{1}{2}L)n=X_2-X_1=S. \tag{11}$$

Here, $S=(X_2-X_1)$, generally, it is on the order of a tenth of a millimeter. Then the response frequency of the system can be calculated by $f=V/S$, where V is moving velocity of the scanning mirror. In our experiments, the moving speed is 10 mm/s. This governs the time response of this kind of sensing system. It takes a long time (say from a few tenths of a second to several seconds) for one measurement value. This is due to the time required to drive the scanning mirror along the translation stage back and forth. It is easy to improve the time response by using high speed translation stage and making the quantity S as short as possible.

If the fiberoptic extensometer is embedded in concrete and the coupler loop length L remains constant, then as the matrix deforms, the optical path of the sensing fiber gauge length L_0 will be varied due to the fiber physical length extension (or compression) and the change of refractive index of the fiber core.

Thus, the average strain of the optical fiber with the gauge length L_0 can be measured by

$$\overline{\epsilon}=\frac{\Delta L_0}{L_0}=\frac{\int dS}{n_{\text{equivalent}}L_0}=\frac{\Delta S}{n_{\text{equivalent}}L_0}, \tag{12}$$

where ΔS can be measured by displacement of the scanning mirror as shown in Fig. 7.

V. WHITE LIGHT INTERFEROMETRIC MULTIPLEXING FIBEROPTIC SENSING SYSTEM

The use of low coherence interferometric multiplexing techniques for distributed strain or temperature sensing in advanced composite or other structural elements has been discussed in several recent articles. For fiberoptic Michelson interferometer systems, multiplexing is a key issue. Schemes based on coherence tuning,[25,26] time division,[27] and spatial-division[28,29] multiplexing methods have been described. Here, we will introduce a fiberoptic coupler[30] multiplexing technique and an improved $1\times N$ star coupler[31] multiplexing scheme, respectively.

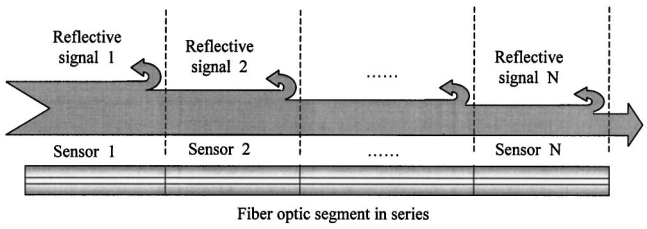

FIG. 10. Reflective signals flow illustration of fiberoptic multiplexing extensometer sensing part.

A. Fiberoptic strain sensors in series

For the case of a fiberoptic strain sensor in series, a sensing arm is formed by a series of finite length fibers as strain sensors. The other arm is a measuring arm in which an optical fiber coupler loop is used as a balance fiber line for matching the length of each sensor of the system. The coupler loop length is nearly equal to the fiber strain gauge length, as shown in Fig. 9.

For the sensing system, we cut and connect a single mode optical fiber, forming N segments. The length of the fiber sensing gauge is $l_1, l_2, \cdots, l_N$, respectively, as shown in Fig. 9. The intensities of optical reflective signals is illustrated by Fig. 10. Assume that l_1 changes to $l_1+\Delta l_1, l_2$ changes to $l_2+\Delta l_2, \cdots, l_N$ changes to $l_N+\Delta l_N$, as distributed stress is applied. Then the distribution of strains is measured as $\epsilon_1=(\Delta l_1/l_1), \epsilon_2=(\Delta l_2/l_2), \cdots, \epsilon_N=(\Delta l_N/l_N)$.

B. Fiberoptic strain sensors in parallel

Using the principle discussed above, we have designed a distributed strain sensing system, in which a $1\times N$ fiberoptic star coupler is used as N distributed strain sensors. The schematic of this distributed sensing system is illustrated in Fig. 11. One of the two branches of the interferometer is connected with a $1\times N$ star coupler, to which N sensing fiber segments are attached. The two ends of each fiberoptic segment are polished and coated with reflectivity R_1 and R_2 as

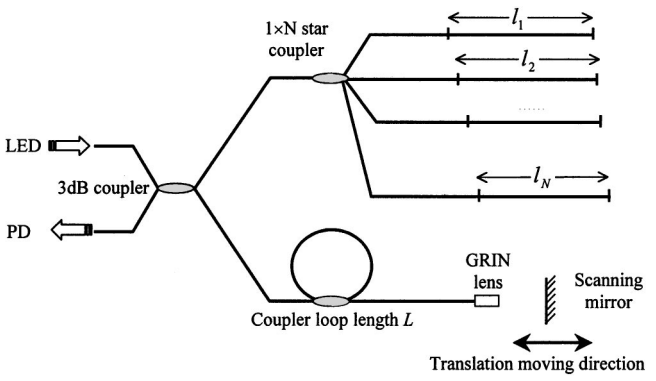

FIG. 11. $1\times N$ star coupler with multiplexing fiberoptic strain sensors in parallel which is improved by a coupler loop.

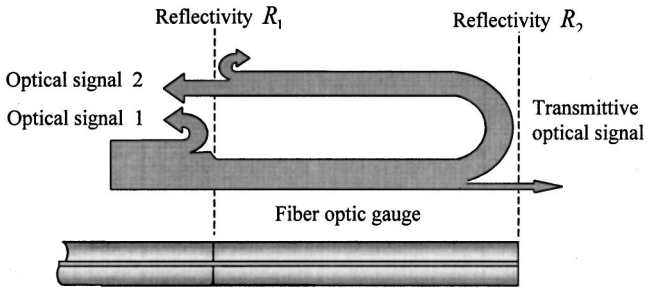

FIG. 12. Reflective and transmissive optical signals flow illustration of each fiberoptic sensor.

shown in Fig. 12. Each of the N fiber arms of the $1\times N$ star coupler function as one strain sensor. The other branch is connected with a coupler loop as a balance measuring arm and is terminated with a GRIN lens. Perpendicular to the GRIN lens, a reflective mirror is mounted on a linear positioning translation stage. It is used for scanning a small distance which can measure the absolute elongation of each sensing fiber length. In Fig. 11, the N length of arms of the $1\times N$ star coupler is equal to $L_1=l_{0_1}+l_1, L_2=l_{0_2}+l_2,\ldots,L_N=l_{0_N}+l_N$, respectively, as N sensors. Assume that l_1 changes to $l_1+\Delta l_1, l_2$ changes to $l_2+\Delta l_2,\ldots,l_N$ changes to $l_N+\Delta l_N$, as distributed stress loads the fiber sensing gauges. Then the distributed strain is measured as $\epsilon(1)=(\Delta l_1/l_1), \epsilon(2)=(\Delta l_2/l_2),\ldots,\epsilon(N)=(\Delta l_N/l_N)$, where $l_i(i=1,2,...,N)$ is embedded gauge length of the sensing optical fiber arms. In order to avoid confusion caused by signal overlap in time, the fiberoptic lengths should satisfy

$$l_i \neq l_j \quad i,j=1,2,...,N, \tag{13}$$

$$n_{\text{eff}}|l_i-l_j|_{\max}<D \quad i,j=1,2,...,N, \tag{14}$$

and

$$n_{\text{eff}}|l_i-l_j|_{\min}>\epsilon_{\max}(k)l_k \quad i,j,k=1,2,...,N. \tag{15}$$

Here, n_{eff} is the effective refractive index of the fiber core. D is the longest motor stage scanning distance and $\epsilon_{\max}(k)$ represents the maximum strain for all of the sensors.

VI. APPLICATION EXAMPLES

A. Concrete strain measurement

The optical fiber extensometer is either structurally embedded during production of a test specimen or attached to the surface of the test piece by way of adhesives. In order to test the performance of the fiberoptic extensometer system, both approaches were tested. Specimen mix proportions by weight of the concrete used in this study were 1:0.5:1.767:1.593 cement: water:sand:aggregate. Type 400 cement and maximum coarse aggregate size passing 9.5 mm and retained on a No. 4 sieve were used. Specimens were cast in $100\times100\times300$ (mm) steel molds. The specimens were cured in a curing room for about four weeks before testing.

1. Testing result of attached on specimen surface

The optical fiber extensometer with length 105.6 mm was attached to the cleaned surface of the concrete specimen by epoxy and localized at the center of the part as shown in Fig. 13. The compression test results compare well with a conventional extensometer plotted in Fig. 14. In this test, the epoxy-glued fiberoptic extensometer de-bonded when the concrete deformation was over 6000 microstrain.

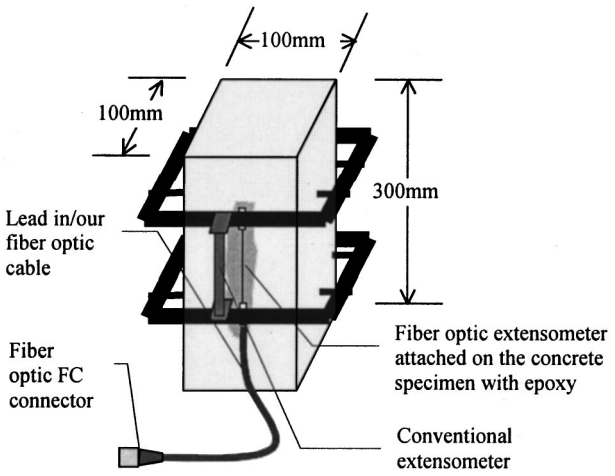

FIG. 13. Concrete specimen for testing.

2. Testing result of embedded in specimen

For an embedded fiberoptic extensometer, a length (104.32 mm) of straight single-mode fiber with polymer protect coating was mounted at the center of steel mold with the aid of a thin string which fixed at the center of mold shells (100×100 mm) as shown in Fig. 15. FC connector was installed and polished at the ends of the extensometer pigtail fiber cable, in order to lead in the light source and lead out the reflective optical signals. The compression test results for the deformation measurement from both fiberoptic extensometer and the average of two external conventional extensometers are plotted in Fig. 16. The deformation measured by the fiberoptic extensometer is in agreement with that from the average of external two traditional extensometers.

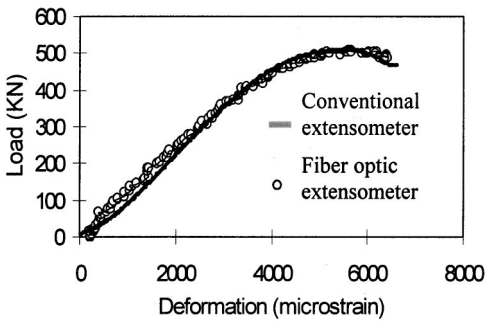

FIG. 14. Concrete compression testing results of fiberoptic extensometer which is attached on the specimen surface compared with conventional extensometer.

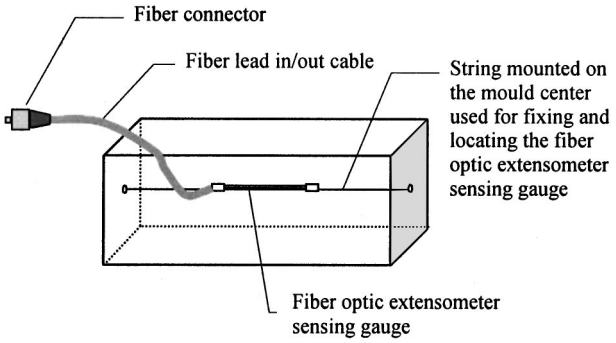

FIG. 15. Installation of fiberoptic extensometer at the concrete mold center aided with a thin string.

B. Temperature

If the white light Michelson fiberoptic extensometer is used as a temperature sensor, the temperature T can be expressed as[32]

$$(T-T_0)=\frac{\Delta S}{L(T_0)n(T_0)[\alpha_T+C_T]}. \tag{16}$$

Here, α_T and C_T are the thermal expansion coefficient and the refractive index temperature coefficient of the optical fiber, respectively. For the standard commercial communication single-mode fiber at wavelength $\lambda=1300$ nm the parameters are $n=1.4681$, $\alpha_T=5.5\times10^{-7}/°C$, $C_T=0.762\times10^{-5}/°$.[21]

To test the sensor performance, the coupler loop with reference fiber length L was coiled and maintained in a chamber at the constant temperature, $T_0=38.5\pm0.1(°C)$, while the fiber sensor coil was heated in an oven. A thermocouple located near the fiber sensor was used to independently monitor its temperature. As the sensor coil was heated or cooled, the optical path variation was recorded. The fiber sensor coil length is 925 mm and the wavelength is 1300 nm. The displacement of the scanning mirror versus the temperature given by the thermocouple over range from 38.5 to 80 °C is plotted in Fig. 17. The relationship is linear as expected from Eq. (16). The system resolution strongly depends on the length of sensing fiber. For this experiment, the sensitivity of the system is measured as $S_T=10.497\,(\mu m/°C)$ and the one standard of deviation value is calculated as $E_S=3.605\,(\mu m)$, thus the resolution of the system is given by

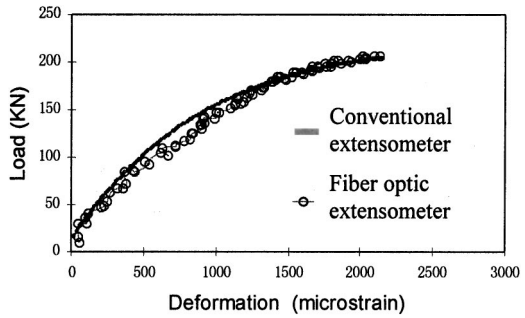

FIG. 16. Concrete compression testing results by fiberoptic extensometer which is embedded in the center of the specimen compared with conventional extensometer.

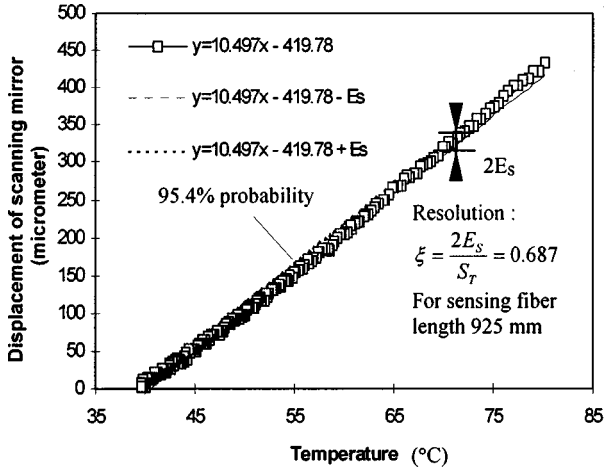

FIG. 17. Fiberoptic sensor temperature calibration.

$$\xi=\frac{2E_S}{S_T}=0.687(°C). \tag{17}$$

C. Dual use for monitoring temperature and measuring CTOD

The embedded optical fiber sensor can be employed as a transducer for measurement of the temperature of fresh concrete at early age. The embedded fibers do not degrade during curing and they bond strongly to the matrix. The permanently embedded fiberoptic sensors offer the opportunity to monitor the strain or displacements associated with the opening of the microcracks of the concrete. In this application, a calibration procedure is developed by which the optical signal is converted to displacements. The temperature test results are compared with a conventional thermocouple. Experiments involved embedding the optical fiber in concrete beams in order to investigate microcrack opening displacement characteristics. Specimens were center-edge notched and the fiberoptic sensor with a gauge length L was embedded at the tip of the notch. This arrangement allowed for direct measurement of displacements associated with the opening of microcracks at the crack tip. Experimental results are presented and crack-tip opening displacement (CTOD) results are compared with crack-opening displacements (COD) measured by conventional transducers at the crack mouth in Ref. 33

To examine the feasibility of using the above fiberoptic sensor system in measuring the temperature in concrete at early ages, and to calculate concrete maturity by using the temperature data, the 24 h temperature monitoring experiments have been done after a length 172 mm fiberoptic sensor embedded in the concrete beam. Near the fiber, a thermocouple was embedded and used to independently monitor its temperature. The testing results of fiberoptic sensor compared with the thermocouple are shown in Fig. 18. After 24 h of temperature monitoring the specimens were cured in a curing room for about four weeks before fracture mechanics testing, then the same optical fiber sensor was used again as a CTOD sensor in the three-point bend tests.[33]

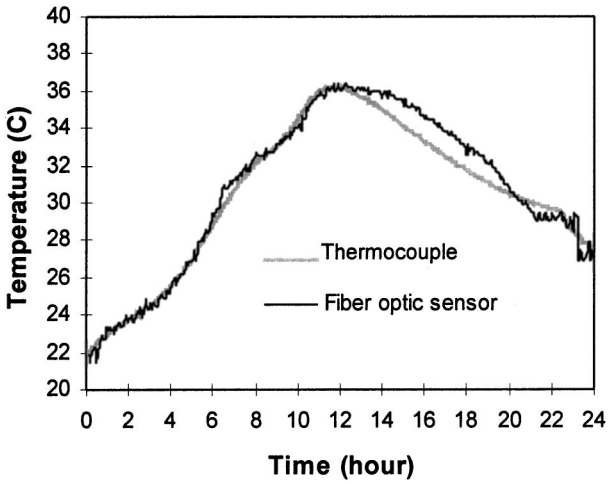

FIG. 18. Temperature monitoring for early fresh concrete specimen.

VII. DISCUSSIONS

Embedded fiberoptic sensors operating on interferometric principles have been considered for measuring strains and temperature inside smart materials and structures. Fiberoptic white light interferometers represent a significant inclusion into the field of structural monitoring. The distinctive feature of these sensors is the use of a scanned reference arm with serial or parallel multiplexing. Since these sensors operate in the spatial domain, they can be multiplexed to monitoring the distribution strain of the structure. In addition to their long-term stability and absolute deformations measurement ability, the fiberoptic sensor used in white light interferometer is simple, durable, and offers sensing gauge length from several centimeters to hundreds meters. It allows unobtrusive attachment to and embedment within a wide variety of materials in composite or concrete structures. It also has been demonstrated that this kind sensor has the potential for multitask, multi-element sensing, allowing (for example) local strain sensing, long-gauge sensing, and sensor self-diagnostics.

ACKNOWLEDGMENTS

This work was supported by the National Nature Science Foundation of China, under Grant No. 59879003, and Science Foundation of Heilongjiang Province for Outstanding Youth, 1999, to Harbin Engineering University and the Research Grant Council of Hong Kong, Grant No. PolyU5160/99E, to The Hong Kong Polytechnic University. The authors acknowledge partial support from the Hong Kong PolyU through project G-V860, G-Y79, and the EE Department.

[1] E. Udd, Rev. Sci. Instrum. **66**, 4015 (1995).
[2] A. D. Kersey, Proc. SPIE **1367**, 2 (1990).
[3] K. Kim, L. Kollar, and G. Springer, J. Compos. Mater. **27**, 1618 (1993).
[4] J. Sirkis, Proc. SPIE **1588**, 26 (1991).
[5] J. Sirkis and H. Haslach, J. Intell. Mater. Syst. Struct. **2**, 3 (1991).
[6] L. P. Kollar and R. J. Van Steenkiste, J. Compos. Mater. **32**, 1647 (1998).
[7] H. Haslach and K. Whipple, Opt. Eng. (Bellingham) **32**, 494 (1993).
[8] G. Hocher, Appl. Opt. **18**, 3679 (1979).
[9] R. Hughes and J. Jarzynski, Appl. Opt. **19**, 98 (1980).
[10] N. Lagakos and Bucaro, Appl. Opt. **20**, 2716 (1981).
[11] A. Dasgupta and J. Sirkis, AIAA J. **30**, 1337 (1992).
[12] G. Carman, R. Averill, K. Reifsnider, and J. Reddy, J. Compos. Mater. **27**, 589 (1992).
[13] S. Case and G. Carman, J. Compos. Mater. **28**, 1452 (1994).
[14] G. Carman and K. Reifsnider, J. Intell. Mater. Syst. Struct. **4**, 88 (1993).
[15] R. J. Van Steenkiste and L. P. Kollar, J. Compos. Mater. **32**, 1681 (1998).
[16] L. B. Yuan and L. M. Zhou, Sens. Actuators A **69**, 5 (1998).
[17] L. B. Yuan and L. M. Zhou, Proceeding of the International Workshop on Fracture Mechanics and Advanced Engineering Materials. Australia, December 8–10, 1999.
[18] T. Li, A. Wang, K. Murphy, and R. Claus, Opt. Lett. **20**, 785 (1995).
[19] D. Inaudi, S. Vurpillot, and S. Lloret, Proc. SPIE **2718**, 251 (1996).
[20] L. B. Yuan, Appl. Opt. **36**, 6246 (1997).
[21] L. B. Yuan, Acta Opt. Sin. **17**, 1713 (1997).
[22] C. D. Butter and G. B. Hocker, Appl. Opt. **17**, 2867 (1978).
[23] D. A. Pinnow, ''ELASTOOPTICAL MATERIALS,'' in *Handbook of Lasers*, edited by R. J. Pressley (CRC, Cleveland, 1971).
[24] L. B. Yuan and L. M. Zhou, Rev. Sci. Instrum. (submitted).
[25] F. Farahi, T. P. Newson, J. D. C. Jones, and D. A. Jackson, Opt. Commun. **65**, 319 (1988).
[26] V. Gusmeroli, M. Martinelli, A. Barberis, and Mariottini, Proceedings of the 9th International Conference on Optical Fiber Sensors, Florence, Italy, 1993, p. 71.
[27] J. L. Santos and D. A. Jackson, Appl. Opt. **30**, 5068 (1991).
[28] Y. J. Rao and D. A. Jackson, Proc. SPIE **2507**, 90 (1995).
[29] L. B. Yuan and F. Ansari, Sens. Actuators A **63**, 177 (1997).
[30] L. B. Yuan, L. Zhou, and W. Jin, Opt. Lett. **25**, 1074 (2000).
[31] L. B. Yuan and L. Zhou, Appl. Opt. **37**, 4168 (1998).
[32] L. B. Yuan, Opt. Laser Technol. **30**, 33 (1998).
[33] L. B. Yuan and F. Ansari, Meas. Sci. Technol. **9**, 261 (1998).